Environ Fluid Mech (2015) 15:905–922
DOI 10.1007/s10652-014-9385-9

ORIGINAL ARTICLE

Unsteady turbulence in expansion waves in rivers and estuaries: an experimental study

Xinqian Leng · Hubert Chanson

Received: 5 March 2014 / Accepted: 11 September 2014 / Published online: 19 September 2014

Abstract A sudden decrease in water depth, called a negative surge or expansion wave, is characterised by a gentle change in free-surface elevation. Some geophysical applications include the ebb tide flow in macro-tidal estuaries, the rundown of swash waters and the retreating waters after maximum tsunami runup in a river channel. The upstream propagation of expansion waves against an initially steady flow was investigated in laboratory under controlled flow conditions including detailed free-surface velocity and Reynolds stress measurements. Both non-intrusive free-surface measurements and intrusive velocity measurements were conducted for relatively large Reynolds numbers with two types of bed roughness. The data showed that the propagation of expansion waves appeared to be a relatively smooth lowering to the water surface. The wave leading edge celerity data showed a characteristic trend, with a rapid acceleration immediately following the surge generation, followed by a deceleration of the leading edge surge towards an asymptotical value: $(\mathrm{U} + \mathrm{V_o})/(\mathrm{g} \times \mathrm{d_o})^{1/2} = 1$ for both smooth and rough bed experiments. The results indicated that the bed roughness had little to no effect, within the experimental flow conditions. Relatively large fluctuations in free-surface elevation, velocity and turbulent shear stress were recorded beneath the leading edge of the negative surge for all flow conditions. The instantaneous turbulent shear stress levels were significantly larger than the critical shear stress for sediment erosion. The present results implied a substantial bed erosion during an expansion wave motion.

Keywords Expansion waves · Negative surges · Turbulence · Scour · Rivers · Estuaries · Tsunami

1 Introduction

In a canal, a sudden increase in water depth is called a positive surge or bore which is a flow discontinuity characterised by a steep front. A sudden decrease in water depth, called a

X. Leng · H. Chanson (✉)
School of Civil Engineering, The University of Queensland, Brisbane, QLD 4072, Australia
e-mail: h.chanson@uq.edu.au
URL: http://www.uq.edu.au/~e2hchans/

Fig. 1 River mouth erosion and damage after tsunami water retreat: aerial view of the tsunami-stricken coastal region near Aceh, Sumatra, Indonesia on 4 January 2005 (US Navy photo by Photographer's Mate 3rd Class Tyler J. Clements)—*note* Lhongka cement factory in background

negative surge, is characterised by a gentle change in free-surface elevation and may occur upstream of an opening gate, as well as downstream of a closing gate [10,18]. It is also called depression, expansion, rarefaction or negative wave [3,34]. Some geophysical applications include the ebb tide flow in macro-tidal estuaries, the rundown of swash waters, and the initial negative wave of a tsunami in a river system or the rundown along the river course after maximum tsunami runup [36]. During the 26 December 2004 and 11 March 2011 tsunami disasters, a number of observations showed that rivers constitute natural breaches in the coastline, thus becoming a natural path for the tsunami waters [6,30,31] (Fig. 1). Their critical funneling role is acknowledged in the extents of inundations, sometimes further aided by the river discharge. While most damage was caused by the advancing tsunami waters, some scour to river mouths as well as structural damage occurred during the tsunami retreat and backrush in the river channels towards the river mouth [21,29,32].

In this contribution, a physical study is presented with a focus on the effects of unsteady turbulence during expansion wave propagation. Detailed free-surface and velocity measurements were performed under controlled flow conditions in a relatively large facility with both smooth and rough boundaries, and the results were ensemble-averaged to predict the expansion wave propagation and associated flow motion. The results highlighted the strong turbulent mixing induced by the negative surge propagation, and the results are discussed in the context of river and estuarine systems.

2 Experimental facility and instrumentation

New experiments were performed in a 12 m long 0.5 m wide horizontal channel, made of smooth PVC bed with 0.30 m high glass sidewalls (Table 1). The experimental flow conditions are summarised in Table 1. The waters were supplied by a constant head tank and the glass wall

Table 1 Experimental investigations of negative surges

$Q\ (m^3/s)$	$\theta\ (°)$	Bed roughness (m)	h (m)	d_o	U (m/s)	$\rho \times \frac{V_o \times d_o}{\mu}$
0.025	0	Smooth PVC	0.045–0.070	0.107–0.23	0.5–1.25	5.0×10^4
		Rough bed (RMA)	0.060–0.073	0.156–0.222	1.01–1.41	
0.035	0	Smooth PVC	0.075–0.090	0.128– 0.181	0.53–0.94	6.8×10^4
		Rough bed (RMA)	0.085–0.092	0.180–0.210	0.83–1.11	

Q initial steady flow rate, $\theta = 0$ horizontal bed slope, d_o, V_o initial flow depth and velocity recorded at sampling location, *U* celerity of negative surge leading edge positive upstream measured at x = 5 m

channel was fed by an intake structure equipped with flow straighteners and meshes followed by a smooth sidewall and bottom convergent. A fast opening tainter gate was located at the downstream end ($x = x_{Gate} = 11.12$ m) where x is the distance from the glass wall channel upstream end (Fig. 2). The opening time was less than 0.15 and 0.2 s, and such a closure time was small enough to have a negligible effect on the surge propagation. Details of the gate are shown in Fig. 2b and photographs of a gate opening sequence are presented in Fig. 4.

The water discharge was measured with an orifice meter calibrated on site. In steady flows, the water depths were measured with rail mounted pointer gauges. The unsteady water depths were recorded with Microsonic™ Mic+25/IU/TC acoustic displacement meters spaced above the channel centreline. The velocity measurements were conducted at x = 5 m with an acoustic Doppler velocimeter (ADV) Nortek™ Vectrino+ equipped with a side-looking head (Fig. 2c). The velocity range was 1.0 m/s herein and the translation of the ADV system in the vertical direction was controlled by a fine adjustment traverse connected to a Mitutoyo™ digimatic scale unit, with an error of less than 0.025 mm. For all the measurements, the ADV control volume was located on the channel centreline at relative elevations $0.07 < z/d_o < 0.65$, where z is the sampling elevation above the bed and d_o the initial flow depth measured at x = 5 m. All the instruments were sampled at 200 Hz. Additional informations were recorded with a Pentax™ K-7 dSLR camera and Sony™ HDR-SR11E HD video camera.

Two types of bed roughness were tested: smooth PVC and rough bed. Some experiments were performed on the smooth PVC bed. For others, the PVC invert was entirely covered with a series of industrial rubber floor mats for $0.075 < x < 11.10$ m (Fig. 3). Figure 3a presents a piece of rubber mat. The hydraulic roughness of smooth and rough beds was tested for a range of steady open channel flow conditions. The bed shear stress was deduced from the measured free-surface profiles and friction slopes. The Darcy–Weisbach friction factor of the smooth PVC bed ranged from 0.020 to 0.050 corresponding to mean equivalent sand roughness height $k_s = 1$ mm. The equivalent Darcy friction factor of the rough bottom was between 0.09 and 0.18, corresponding to $k_s = 39$ mm on average which was comparable to the roughness element size.

The experimental flow conditions are summarised in Table 1. The key features herein were the detailed measurements under controlled flow conditions for relatively large discharges and Reynolds numbers, combined with systematic experiments of both smooth and rough bottoms. Further all the experiments were repeated 25 times and both free-surface and velocity data were ensemble-averaged. As part of preliminary investigations, the gate opening was filmed and the repeatability of the experiments was tested with several operators. The video observations showed no effect of the gate operator and total gate opening time for opening times less than 0.25 s. The finding was consistent with the results of Lauber [16] showing

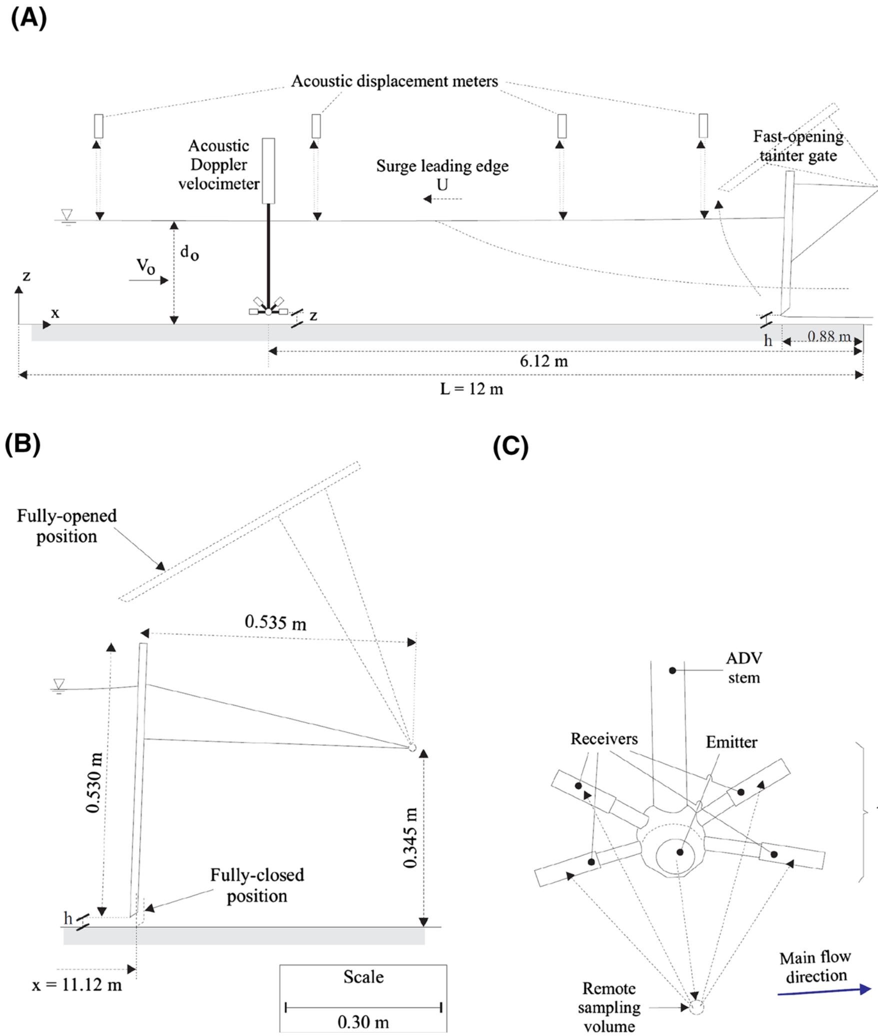

Fig. 2 Sketch of experimental facility. **a** Flume and instrumentation mounting. **b** Dimensioned sketch of tainter gate. **c** Sketch of ADV side-looking head

no effect of gate opening for an opening time less than 0.2 s. A sensitivity analysis was conducted to test the effects of number of experimental runs in terms of the free-surface properties, longitudinal velocity component and tangential stress $\overline{v_x \times v_z}$ with the rough bed configuration. The results showed that, during the propagation of the negative surge (incl. the leading edge passage), the time-variations of the free-surface elevation, free-surface fluctuations, longitudinal velocity median, velocity fluctuations and median tangential stress were little affected by the number of runs for a minimum of 15 to 20 runs. A fuller discussion on the ensemble-averaging method and data presentation is developed in the Appendix.

Further details on the experimental facility and instrumentation were reported in Leng and Chanson [17].

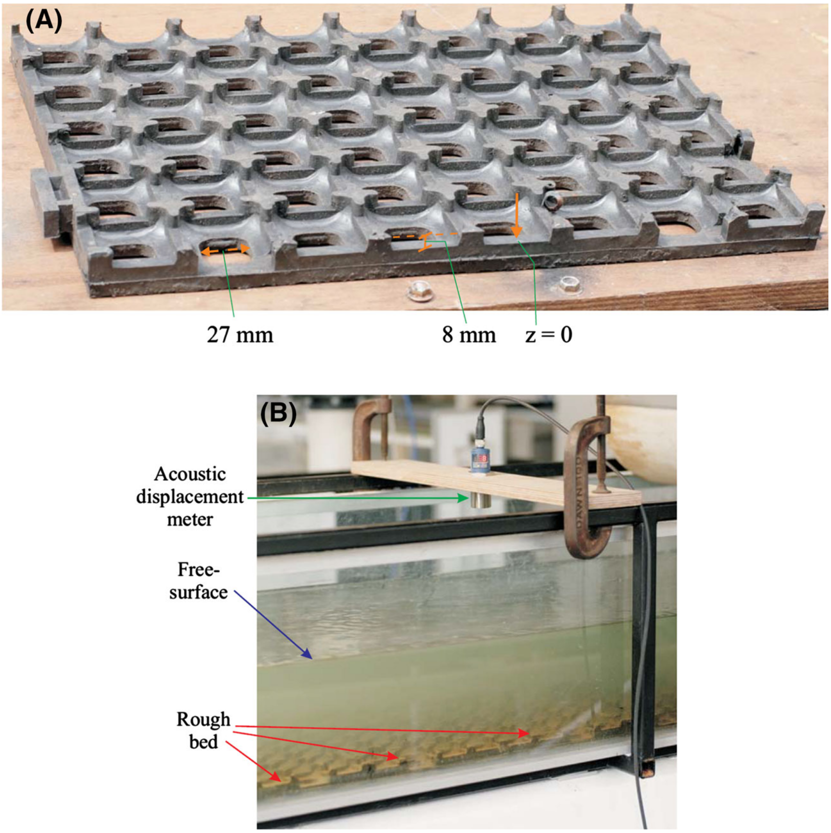

Fig. 3 Rough bed configuration. **a** Details of a rubber matt element with dimensions. **b** Initially steady flow at x = 5 m: Q = 0.025 m^3/s, d_o = 0.154 m, rough bed configuration, flow direction from left to right—*note* acoustic displacement sensor mounted above the channel

3 Basic observation

3.1 Free-surface patterns and measurements

Visual, photographic and video observations showed that the rapid gate opening led to a steep drop of the water surface next to and immediately upstream of the gate (Fig. 4). Figure 4 shows a sequence of photographs of the gate opening and initial stages of the expansion wave. In Fig. 4, Q is the initially steady flow rate and h is the undershoot gate opening (before rapid opening). In both Figs. 2a, b and 4, the initially steady flow discharge runs from left to right, and the negative surge (i.e., expansion wave) propagates from right to left. The observations highlighted the rapid gate opening in less than 0.2 s and the negative wave formation. The free-surface profile exhibited a smooth shape, within one second, despite some limited disturbance induced by the gate motion. The instantaneous free-surface profile presented a very flat surface when the surge propagated upstream. All the visual observations indicated the gentle gradual lowering of the free-surface during the negative surge motion. The upstream propagation of the surge leading edge was barely perceptible, but immediately after gate opening. The free-surface patterns were identical for both smooth and rough bed

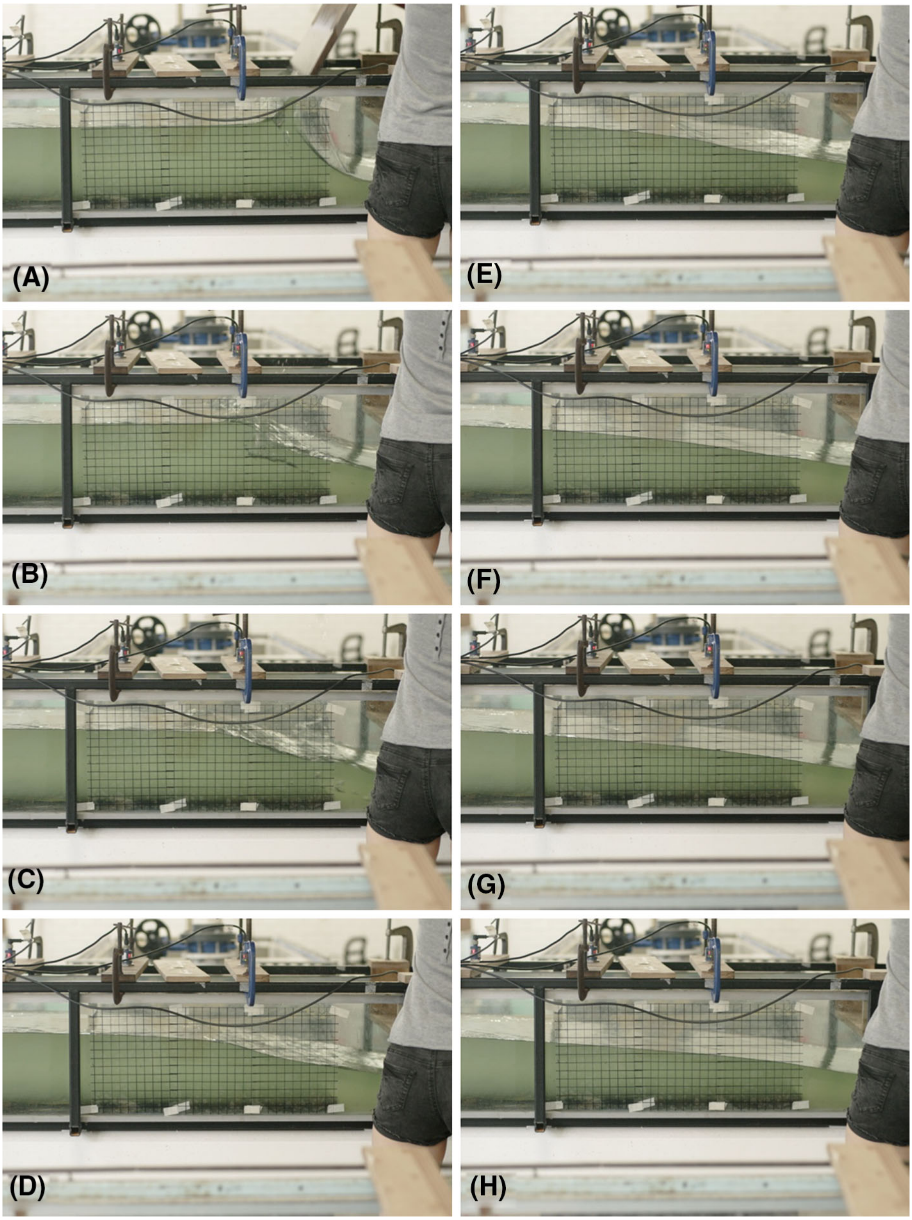

Fig. 4 Visual observations of expansion wave immediately upstream of the gate ($x_{Gate} = 11.12$ m)—flow conditions: $Q = 0.0345$ m^3/s, $d_o = 0.182$ m, $h = 0.075$ m, rough bed (RMA)—from *top* to *bottom* then *left* to *right* $t = 0$, 0.19, 0.38, 0.57, 0.76, 0.95, 1.14, 1.33 s

experiments and for all experiments (Table 1). They were further consistent with the earlier observations of Reichstetter and Chanson [25] on smooth bed.

The entire wave process may be divided into a short generation phase followed by a gradually-varied flow motion. The former encompassed the gate opening and the first initial instants. The gate opening was associated with a rapid drop in water elevation immediately

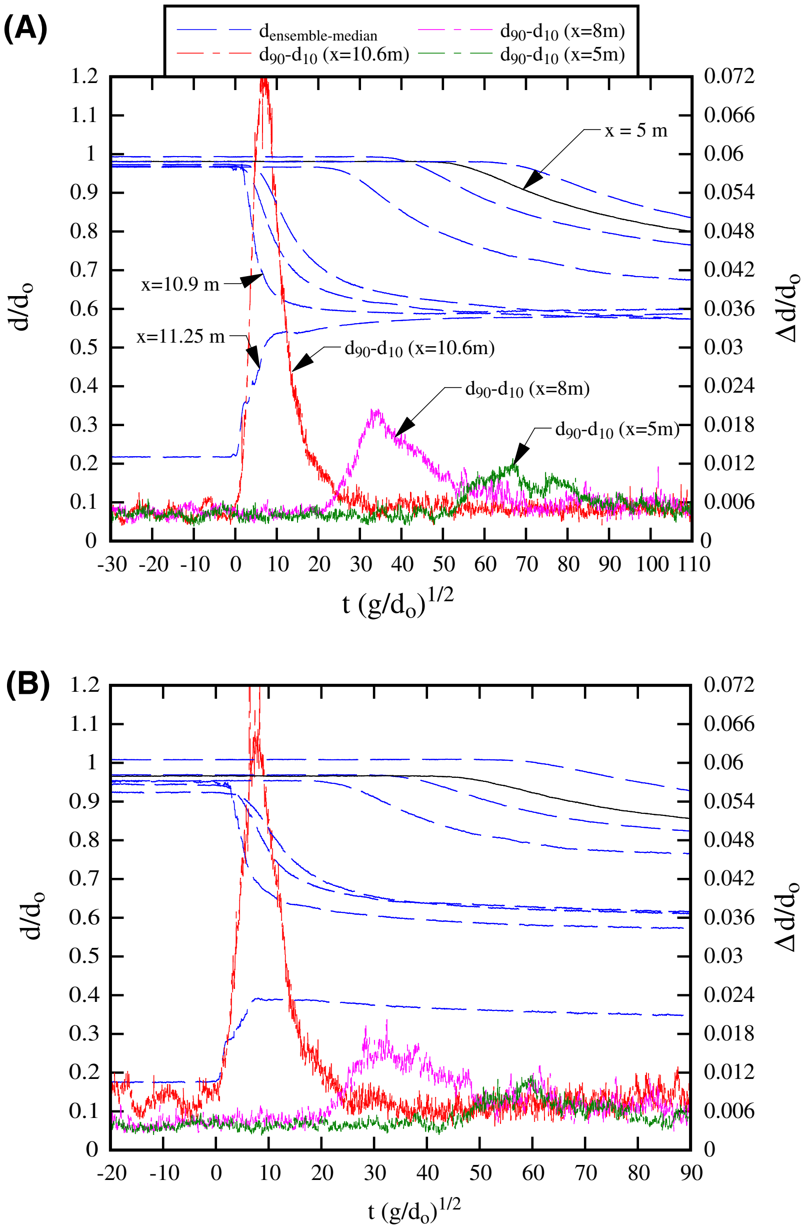

Fig. 5 Ensemble-averaged median water depth and water surface fluctuations (difference between ninth and first deciles) $(d_{90} - d_{10})$ during the expansion wave propagation—water depth data at x = 11.25, 10.9, 10.6, 10.3, 8, 6.5, 5 and 3.5 m; $(d_{90} - d_{10})$ data at x = 10.6, 8 and 5 m; same legend for both graphs. **a** Smooth bed, Q = 0.0254 m^3/s, d_o = 0.154 m, h = 0.055 m. **b** Rough bed, Q = 0.0345 m^3/s, d_o = 0.182 m, h = 0.092 m

upstream of the gate as well as a rapid increase in water surface elevation immediately downstream of the gate which corresponded to the downstream propagation of a positive surge. Both processes are illustrated in Fig. 5 showing the time variations of the ensemble

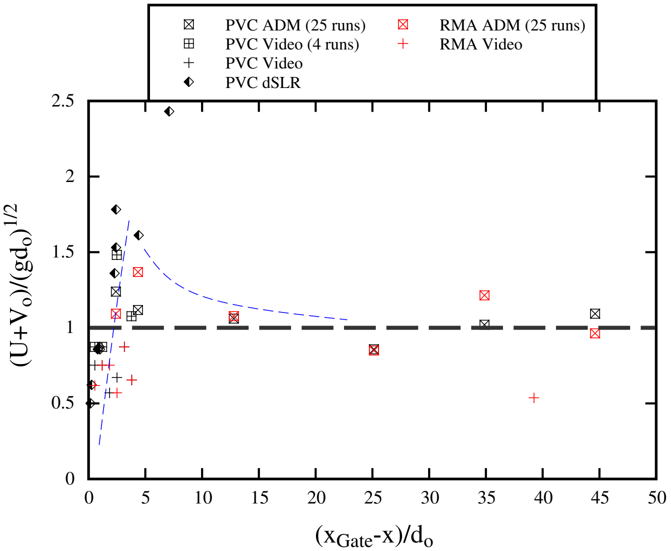

Fig. 6 Dimensionless celerity of the expansion wave leading edge as function of the distance from the gate—comparison between ensemble-averaged acoustic displacement meter (ADM) data (25 runs), video data [single run and ensemble-average (4 runs)], and dSLR data (single run)—flow conditions: $Q = 0.0254\,m^3/s$, $d_o = 0.154\,m$, smooth and rough beds

median water depth, where the time origin $t = 0\,s$ corresponded to the gate opening. The effects of the gate opening were clearly seen for the data of the two sensors located either side of the gate: i.e., $x = 11.25$ and $10.9\,m$. Following the generation phase, all the free-surface data highlighted the smooth free-surface profile at the surge leading edge associated with an unsteady gradually-varied flow motion. The free-surface curvature and slope were larger close to the gate than further upstream, but the radius of curvature was quantitatively large, implying quasi-hydrostatic pressure distributions. Figure 5 presents several ensemble-averaged free-surface measurements at several longitudinal locations. Both the ensemble median and the difference between the ninth and first deciles ($d_{90} - d_{10}$) are presented. The latter ($d_{90} - d_{10}$) characterised the instantaneous free-surface fluctuations at the sensor location. For all experiments, the data showed relatively large fluctuations in free-surface elevations associated with the propagation of the surge leading edge (Fig. 5). The maximum free-surface fluctuations decreased exponentially with increasing distance from the gate as illustrated in Fig. 5a, b.

3.2 Expansion wave celerity

The celerity of the expansion wave leading edge was recorded using a combination of photographic, video and acoustic displacement meter data. Figure 6 presents a typical data set: both ensemble-averaged and single run data are included. Overall the data showed the same distinctive trend for both smooth and rough bed configurations and for all experimental flow conditions. Immediately after the gate opening, the negative wave formed very swiftly and the celerity of its leading edge increased very rapidly with distance, reaching a maximum dimensionless value $(U + V_o)/(g \times d_o)^{1/2}$ in excess of two, where U is the wave celerity positive upstream and V_o is the initial flow velocity at $x = 5\,m$ (Fig. 6). This acceleration phase corresponded to the expansion wave generation phase illustrated in Fig. 4. Further upstream, the negative wave leading edge decelerated and propagated in a more gradual manner. Its celerity decreased with increasing distance from the gate towards an asymptotical value $(U+V_o)/(g \times d_o)^{1/2} = 1$ for both smooth and rough bed configurations and all investigated flow conditions (Table 1). This asymptotical limit was equal to the analytical solution of the St. Venant equations for a horizontal frictionless rectangular channel [5,10]. The present results showed that the bottom roughness had no effect on the celerity of the negative surge, within the experimental flow conditions (see below). Altogether the findings were consistent with the observations of Reichstetter and Chanson [25], albeit their experiments were conducted only for one discharge on smooth PVC invert.

3.3 Discussion

Expansion waves in open channels may be analysed using the St. Venant equations. The St. Venant equations are one-dimensional unsteady open channel flow equations characterising the variations with time of the water depth d and flow velocity V:

$$\frac{\partial A}{\partial t} + \frac{\partial Q}{\partial x} = 0, \tag{1}$$

$$\frac{1}{g} \times \left(\frac{\partial V}{\partial t} + V \times \frac{\partial V}{\partial x}\right) + g \times \frac{\partial d}{\partial x} - S_o + S_f = 0, \tag{2}$$

where x is the longitudinal co-ordinate positive downstream, t is the time, A is the flow cross-section area, Q is the water discharge, B is the free-surface width, g is the gravity acceleration, S_o is the bed slope and S_f is the friction slope:

$$S_f = \frac{f}{D_H} \times \frac{V^2}{2 \times g}, \tag{3}$$

with f the Darcy–Weisbach friction factor and D_H the equivalent pipe diameter also called hydraulic diameter. The dynamic equation may be simplified when some terms become small [5,19]. Within the experimental flow conditions, the friction slope was found to 10–100 times smaller than the first three terms of the dynamic equation during the passage of the expansion wave leading edge. Thus the influence of the friction source term was small, as observed experimentally herein.

The free-surface data highlighted some relatively large free-surface fluctuations $(d_{90}-d_{10})$ for a short duration during the propagation of the negative surge which must be associated with some energy. The total energy of these free-surface fluctuations is a combination of the potential energy due to the water elevation above the ensemble mean level, and the kinetic energy due to the fluid motion. In a negative surge, the velocity distributions are complex and the kinetic energy cannot be analytically deduced. Instead the potential energy per surface area was estimated as the integral of the weight of water above the (ensemble) mean water level times the distance to the centroid [18] and used herein as a surrogate of the total fluctuation energy. The potential energy per surface area P_E was estimated as:

$$P_E = \int_0^{t_1} \frac{1}{2} \times \rho \times g \times (d_{90} - d_{10})^2 \times dt, \tag{4}$$

where t_1 is the negative surge sampling duration. Note that Eq. (4) assumes a two-dimensional surge propagation. Figure 7 shows some typical results for both smooth and rough bed data. Overall the dimensionless wave energy decreased exponentially with increasing distance

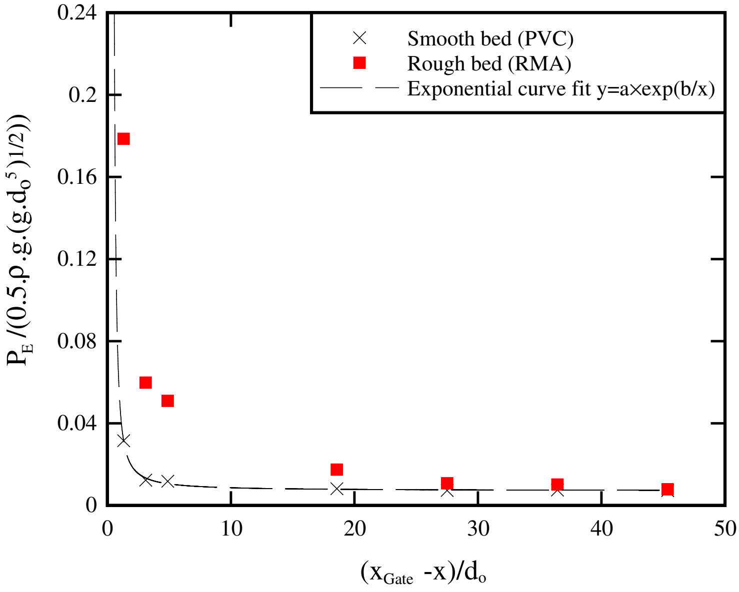

Fig. 7 Potential energy per unit area P_E of free-surface fluctuations during negative wave as a function of distance from gate—flow conditions: $Q = 0.0345\,m^3/s$, $d_o = 0.18\,m$, smooth and rough beds

from the gate for all flow conditions on both smooth and rough beds. While the potential energy per unit area data were large close to the gate, the free-surface fluctuation energy tended to yield close results for both smooth and rough bed experiments further upstream (Fig. 7).

4 Velocity measurements

Detailed unsteady velocity measurements were conducted for two flow rates on both smooth and rough bed configurations (Table 1). The instantaneous velocity data showed a marked acceleration of the flow as the expansion wave leading edge passed over the sampling volume (Fig. 8). Figure 8 presents some typical instantaneous velocity data for a single run on the rough bed. In Fig. 8, each graph includes the three velocity components (V_x, V_y, V_z) as well as the instantaneous water depth at x = 5, 8 and 10.6 m, where V_x is the longitudinal velocity component positive downstream, V_y is the transverse velocity component positive towards the left sidewall and V_z is the vertical velocity component positive upwards. At x = 5 m, the data showed the gradual lowering of the water surface associated with the acceleration of the flow (Fig. 8). All the velocity components tended to show relatively larger fluctuations shortly after the passage of the negative surge leading edge: e.g., at $t \times (g/d_o)^{1/2} \approx 40$–60 in Fig. 8. Overall similar results were observed for all elevations and bed configurations.

The free-surface and velocity measurements were conducted 25 times and the results were ensemble-averaged. The ensemble-averaged velocity data were analysed in terms of the median velocity V_{median} and the instantaneous velocity fluctuations taken herein as the difference between the ninth and first deciles ($V_{90} - V_{10}$; Fig. 9). Figure 9 presents some typical results. All the data results showed that the propagation of the negative surge was

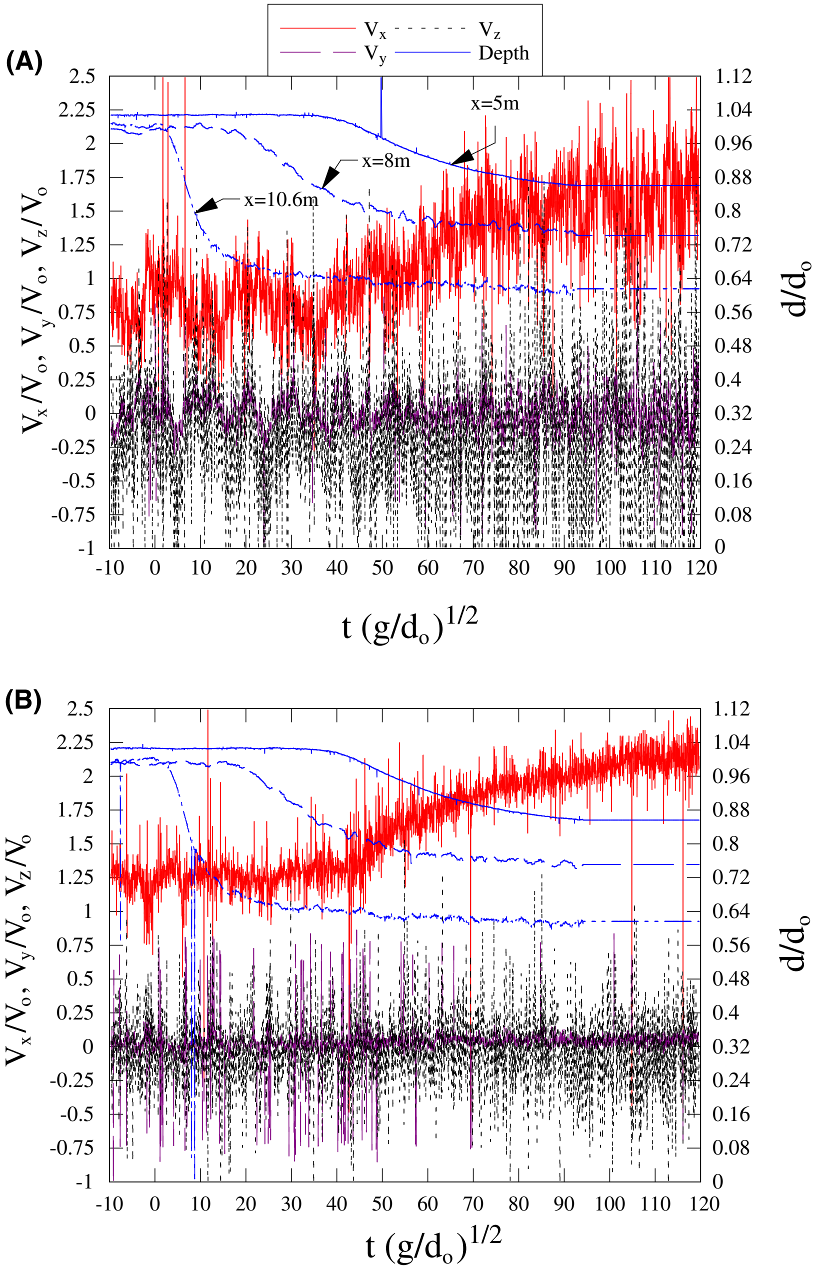

Fig. 8 Instantaneous free-surface velocity data beneath a expansion wave—flow conditions: Q = 0.0345 m^3/s, x = 5 m, d_o = 0.2013 m, V_o = 0.343 m/s, h = 0.085 m, rough bed (RMA), single run—water depths at x = 10.6, 8.0, and 5.0 m, velocity data at x = 5 m; same legend for both graphs. **a** $z/d_o = 0.24$. **b** $z/d_o = 0.69$

associated with some longitudinal acceleration, as well as some increase in velocity fluctuations, at all vertical elevations ($0.06 < z/d_o < 0.9$) on both smooth and rough beds for all velocity components. The velocity data suggested that the acceleration was comparatively

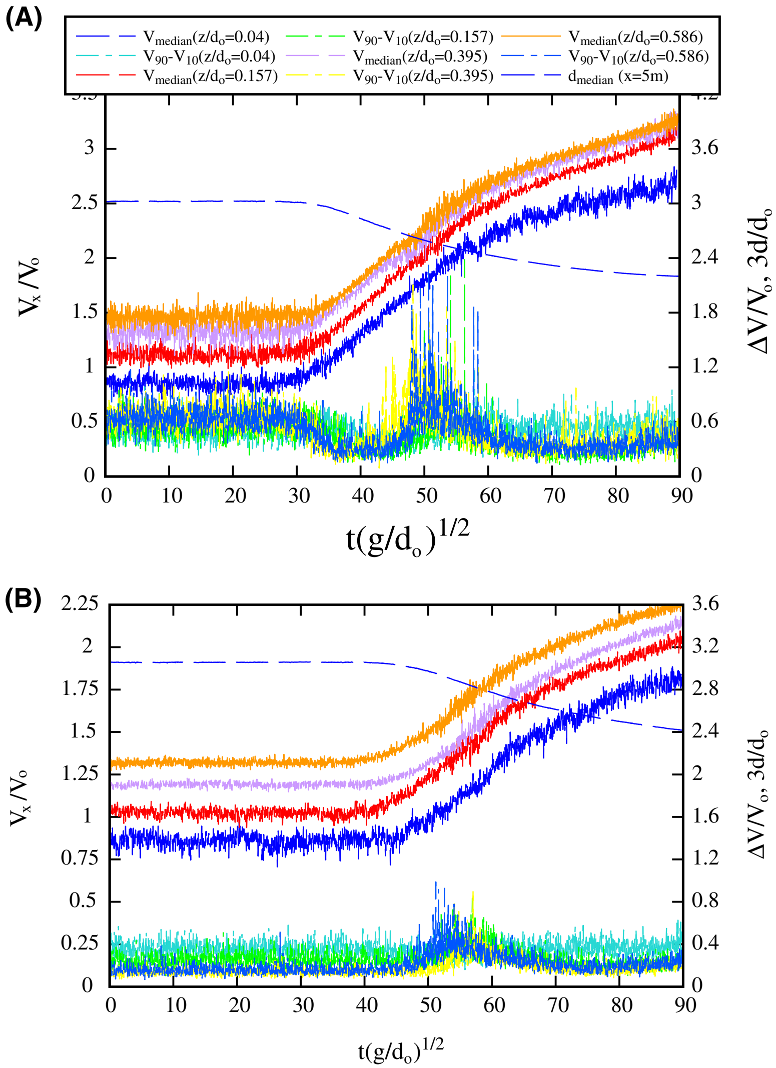

Fig. 9 Ensemble median water depth and longitudinal velocity and velocity fluctuation ($V_{90} - V_{10}$) during a expansion wave—smooth bed (PVC), 25 runs, $z/d_o = 0.04$, 0.157, 0.395 and 0.586—V_x data offset by 0.1 for the three highest elevations; same legend for both graphs. **a** $Q = 0.0245\,m^3/s$, $x = 5\,m$, $d_o = 0.21\,m$, $h = 0.045\,m$. **b** $Q = 0.0345\,m^3/s$, $x = 5\,m$, $d_o = 0.20\,m$, $h = 0.066\,m$

larger in the upper water column (i.e., $z/d_o > 0.38$). Close to the free-surface, some negative vertical velocity component was observed and the result was consistent with the water surface drop following the passage of the surge leading edge, ending to zero at the invert ($z = 0$) as implied by the no-flow-through boundary condition.

Some distinct peaks in velocity fluctuations ($V_{90} - V_{10}$) were seen at higher vertical elevations ($z/d_o \geq 0.04$) on both bottom configurations following the passage of the surge leading edge: e.g., about $t \times (g/d_o)^{1/2} \approx 45$–60 in Fig. 9. For the same vertical elevation, the maximum velocity fluctuations were comparatively smaller on the rough bed compared to

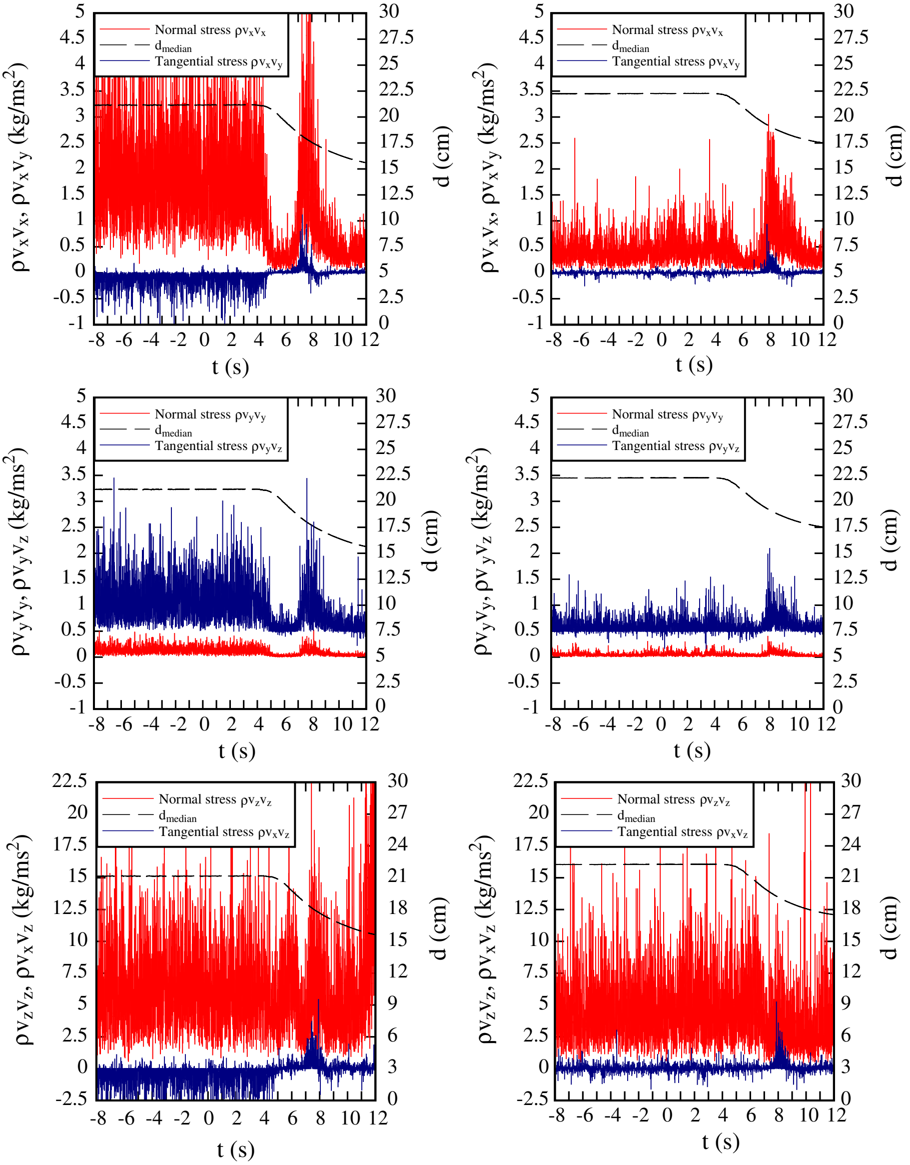

Fig. 10 Ensemble median turbulent Reynolds stresses in expansion wave—flow conditions: $Q = 0.0254\,m^3/s$, $x = 5\,m$, $z/d_o = 0.586$. **a**, *Left* smooth bed, $d_o = 0.21\,m$, $h = 0.045\,m$. **b**, *Right* rough bed, $d_o = 0.22\,m$, $h = 0.064\,m$

those recorded on the smooth PVC bed. This might be associated with the higher turbulence levels and additional turbulence production above the rough bed masking the surge generated turbulent fluctuations. On both smooth and rough beds, the unsteady velocity fluctuations differed substantially from steady flow conditions, with higher fluctuation levels of all three components.

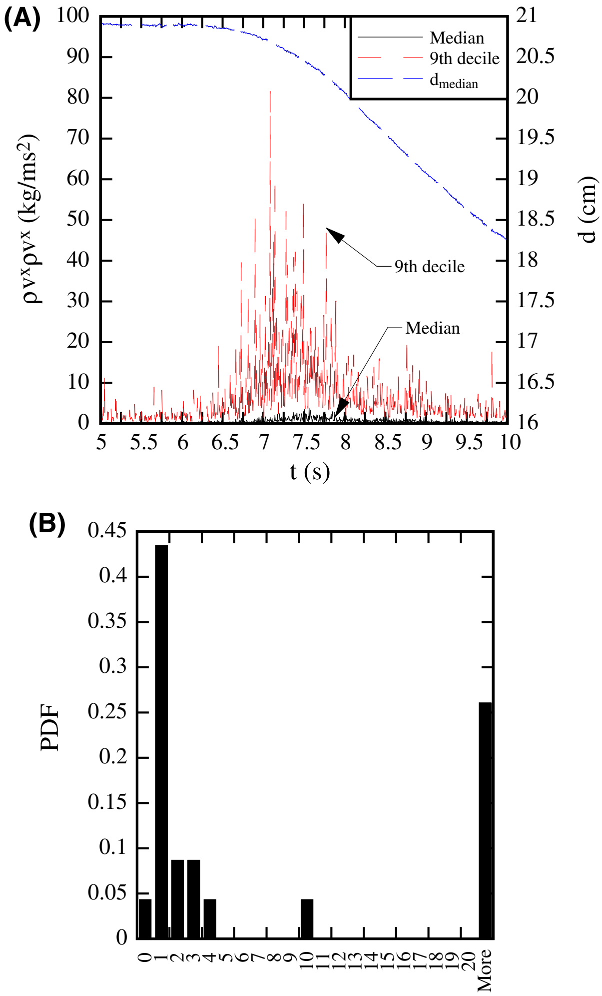

Fig. 11 Instantaneous ensemble median normal stress $\rho \times v_x \times v_x$ and depth during the expansion wave leading edge passage—comparison between the instantaneous ensemble median and ninth decile of normal stress $\rho \times v_x \times v_x$—flow conditions: $Q = 0.0345\,m^3/s$, $x = 5\,m$, $d_o = 0.205\,m, z/d_o = 0.628$, PVC bed. **a** Time variation of instantaneous ensemble median and ninth decile of normal stress $\rho \times v_x \times v_x$. **b** Normalised probability distribution function of normal stress $\rho \times v_x \times v_x$ at $t = 7.278\,s$

The Reynolds stresses were calculated based upon the deviation between the measured velocity and the ensemble median. Typical results are presented in Fig. 10 for both smooth and rough beds. Figure 10a, b present the dimensional ensemble median water depth and Reynolds stress components as functions of time. All the data showed consistently that the passage of the negative surge was associated with large turbulent stress levels as well as large fluctuations in ensemble median turbulent stresses at all vertical elevations. The magnitude of the Reynolds stress tensor components was larger than in the initially steady flow.

5 Discussion

Herein maximum medians of instantaneous shear stress were recorded up to 5–10 Pa, independently of the bed roughness (Fig. 10). However much larger individual levels of shear stress were observed as illustrated in Fig. 11a comparing the median stress data with the ninth decile of the ensemble. Figure 11b shows further the probability distribution function of the normal stress component $\rho \times v_x \times v_x$ at $t = 7.278\,s$ for the data set shown in Fig. 11a. Both

Figs. 10 and 11 are presented in a dimensional form to show the magnitude of Reynolds shear stress. Altogether the experimental data showed maximum instantaneous normal stress data in excess of 100 Pa and maximum instantaneous tangential stress amplitude larger than 50 Pa. These results implied that the negative surge had the potential to scour a natural mobile bed made of fine cohesive and non-cohesive materials. For non-cohesive sediments, the Shields diagram predicts a critical shear stress for sediment motion onset of about $(\tau_o)_c$=0.1–0.5 Pa for fine sand particles with sizes between 0.1 and 1 mm [8,14]. For cohesive sediments, the material yield stress is related to the minimum boundary shear stress required to erode and re-suspend the sediments [22,33]. Recent field observations indicated mud yield stress between 5 and 60 Pa [2,7,26]. These values may be compared to critical shear stress data for cohesive sediment erosion between 0.1 and 10 Pa [13,27].

In the present study, the instantaneous Reynolds stress levels were one to two orders of magnitude larger than the critical threshold $(\tau_o)_c$ for sediment transport for both cohesive and non-cohesive materials. The results indicated that, at the laboratory scale, the negative surge could scour fine sediment particles and advect them downstream into suspension during the acceleration phase. Based upon an undistorted Froude similitude, the shear stress scaling ratio equals the geometric scaling ratio [11,20]. Thus, in a practical application, such as a river channel with greater water depths than the present experiments, mobile bed scour erosion may occur when a negative surge propagates upstream, before the particles are entrained downstream in the accelerated backrush flow. The process might explain the intense erosion observed during the backrush of tsunami waters in rivers and estuaries.

During recent tsunami disasters, a number of observations indicated the inundation caused by tsunami waters following river courses, as well as major damage caused during the backrush along the estuarine channels. During the 2010 Chilean tsunami, retreating tsunami currents approached 6–7 m/s at the Ventura Harbor channel (California) causing significant scour at the mouth of the harbour [35]. During the 2011 Tohoku earthquake and tsunami, significant erosion and scour of the subsurface soil deposits was caused by repetition of inflow and retreat of the tsunami in river courses [12]. Hazarrika et al. [9] reported major damage to river embankments during the backrush: "the overflowing tsunami while retreating made a concentrated attack on the weak part of the structure". Sasaki et al. [28] similarly reported significant erosion of river dykes upon retreat of the tsunami water. Tanaka et al. [32] discussed the drainage of river courses during the retreating tsunami phases. They observed that the backrush flow caused shoreline breaching at old river mouth locations: "the breaching occurred due to the strong return flow through the drainage" channels [32].

6 Conclusion

The present study provided some new insights into the physical processes associated with expansion waves (i.e., negative surges) and their potential to scour river bed and river mouth. Based upon a laboratory study under controlled flow conditions, the data showed that the upstream propagation of negative surges appeared visually to be a relatively smooth lowering to the water surface. The surge leading edge celerity data presented a characteristic trend, with a rapid acceleration immediately following the gate opening, followed by the deceleration of the leading edge surge celerity towards an asymptotical value: $(U + V_o)/(g \times d_o)^{1/2} = 1$ for both smooth and rough bed experiments. The present results indicated that the bed roughness had little effect, within the experimental flow conditions. Relatively large free-surface fluctuations and turbulent velocity fluctuations were recorded beneath the leading edge of the expansion wave for all flow conditions. Large mean and instantaneous turbulent shear stress levels were measured, significantly larger than in the initially steady flow, and typically greater than the critical shear stress for bed scour. The present results showed that bed erosion will occur as the wave leading edge propagates upstream into a river, thus placing the sediment bed material into suspension before it is advected downstream in the accelerated rundown flow. Environmental applications of the work encompass the ebb tide flow in a macro-tidal estuary and the backflow of tsunami waters along a river course.

Acknowledgments The authors thank Professor Hitoshi Tanaka, Tohoku University (Japan) for his advice and relevant information, as well as Dr. Mario Franca, EPFL (Switzerland) and Professor Fabian Bombardelli, University of California Davis (USA) for their helpful comments. The authors acknowledge the technical of Jason Van Der Gevel and Matthews Stewart, School of Civil Engineering at the University of Queensland. The financial support of the Australian Research Council (Grant DP120100481) is acknowledged.

7 Appendix: on ensemble-averaging

A fundamental challenge was the flow unsteadiness associated with the very-rapidly-varied unsteady motion during the surge propagation. While phase-averaging can be easily performed in periodic flows (e.g., [4,23]), the technique is not suitable to very-rapidly-varied flows including the present study. Instead the experiments must be repeated in a carefully controlled manner and the results must be ensemble-averaged [1,15]. Herein each experiment was conducted 25 times, although it is acknowledged that the number of repeated runs was relatively limited. A sensitivity analysis was performed on the effects of experiment number in terms of the free-surface properties, longitudinal velocity component and tangential stress $\overline{v_x \times v_z}$ for the rough bed configuration. The results showed that, during the propagation of the negative surge, including the leading edge passage, the time-variations of the free-surface elevation and free-surface fluctuations ($d_{90} - d_{10}$) were basically independent of the number of experiments for a minimum of 15 runs. And the time-variations of the longitudinal velocity component and velocity fluctuations ($V_{90} - V_{10}$) were basically independent of the number of experiments for a minimum of 15 runs. Similarly the time variations of the median tangential stress $\overline{v_x \times v_z}$ were little affected by the number of runs for a minimum of 20 runs. Altogether it is believed that the selection of 25 repeats was a reasonable compromise and may be compared with the results of Perry et al. [24] who needed 10 samples for convergence of the phase-averaged data. Herein the data were presented in terms of the median and decile difference values. This approach is commonly used in statistics with small to medium size data sets for which the mean and standard deviation values may be biased by outliers.

References

1. Bradshaw P (1971) An introduction to turbulence and its measurement. Pergamon Press, Oxford. The Commonwealth and International Library of Science and Technology Engineering and Liberal Studies, Thermodynamics and Fluid Mechanics Division
2. Brown R, Chanson H (2012) Suspended sediment properties and suspended sediment flux estimates in an urban environment during a major flood event. In: Water resources research, AGU, vol 48, Paper W11523. doi:10.1029/2012WR012381
3. Bryson AE (1969) Film notes for waves in fluids. National Committee in Fluid Mechanics Films, No. 21611
4. Cantwell BJ (1976) A flying hot wire study of the turbulent near wake of a circular cylinder at a Reynolds Number of 140,000. PhD Thesis, California Institute of Technology, Pasadena
5. Chanson H (2004) Environmental hydraulics of open channel flows. Elsevier-Butterworth-Heinemann, Oxford

6. Chanson H, Lubin P (2013) Chapter 3: mixing and sediment processes induced by tsunamis propagating upriver. In: Cai T (ed) Tsunamis: economic impact, disaster management and future challenges. Nova Science Publishers, Hauppauge, pp 65–102
7. Chanson H, Reungoat D, Simon B, Lubin P (2011) High-frequency turbulence and suspended sediment concentration measurements in the Garonne River tidal bore. Estuar Coast Shelf Sci 95(2–3):298–306. doi:10.1016/j.ecss.2011.09.012
8. Graf WH (1971) Hydraulics of sediment transport. McGraw-Hill, New York
9. Hazarrika H, Kasama K, Suetsugu D, Kataoka S, Yasufuku N (2013) Damage to geotechnical structures in waterfront areas of northern Tohoku due to the March 11, 2011 tsunami disaster. Indian Geotech J 43(2):137–152
10. Henderson FM (1966) Open channel flow. MacMillan Company, New York
11. Hughes SA (1993) Physical models and laboratory techniques in coastal engineering. In: Advanced series on ocean Engineering, vol 7. World Scientific Publishing, Singapore
12. Ishihara K, Araki K, Bradley B (2011) Characteristics of liquefaction-induced damage in the 2011 Great East Japan earthquake. In: Proceedings of the international conference on geotechnics for sustainable development (Geotec Hanoi 2011), Hanoi, Vietnam, 6–7 October
13. Jacobs W, Le Hir P, Van Kesteren W, Cann P (2011) Erosion threshold of sand–mud mixtures. Cont Shelf Res 31(Supplement):S14–S25. doi:10.1016/j.csr.2010.05.012
14. Julien PY (1995) Erosion and sedimentation. Cambridge University Press, Cambridge
15. Kim J, Moin P (1986) The structure of the vorticity field in turbulent channel flow. J Fluid Mech 162:339–363
16. Lauber G (1997) Experimente zur Talsperrenbruchwelle im glatten geneigten Rechteckkanal ('Dam break wave experiments in rectangular channels'). PhD Thesis, VAW-ETH, Zürich (in German)
17. Leng X, Chanson H (2014) Propagation of negative surges in rivers and estuaries: unsteady turbulent mixing and the effects of bed roughness. Hydraulic Model Report No. CH93/13. School of Civil Engineering, The University of Queensland, Brisbane
18. Liggett JA (1994) Fluid mechanics. McGraw-Hill, New York
19. Mahmood K, Yevdjevich V (1975) Unsteady flow in open channels, 3 volumes. WRP Publications, Fort Collins
20. Novak P, Cabelka J (1981) Models in hydraulic engineering. Physical principles and design applications. Pitman Publishing, London
21. Okayasu A, Shimozono T, Yamazaki H, Ngai T, Sato S (2013) Severe erosion of sandbar at Unosumai River mouth, Iwate, due to 2011 Tohoku tsunami. In: Proceedings of the coastal dynamics 2013, Arcachon, France, pp 1311–1320
22. Otsubo K, Muraoko K (1988) Critical shear stress of cohesive bottom sediments. J Hydraul Eng ASCE 114(10):1241–1256
23. Perry AE, Watmuff JH (1981) The phase-averaged large-scale structures in three-dimensional turbulent wakes. J Fluid Mech 103:33–61
24. Perry AE, Lim TT, Chong MS (1980) The instantaneous velocity fields of coherent structures in coflowing jets and wakes. J Fluid Mech 101(2):243–256
25. Reichstetter M, Chanson H (2013) Negative surges in open channels: physical and numerical modeling. J Hydraul Eng ASCE 139(3):341–346. doi:10.1061/(ASCE)HY.1943-7900.0000674
26. Reungoat D, Chanson H, Caplain B (2014) Sediment processes and flow reversal in the undular tidal bore of the Garonne River (France). Environ Fluid Mech 14(3):591–616. doi:10.1007/s10652-013-9319-y
27. Sanchez M, Levacher D (2008) Erosion d'une vase de l'estuaire de la Loire sous l'action du courant ('erosion of a mud from the Loire estuary by a flow'). Bull Eng Geol Environ 67:597–605. doi:10.1007/s10064-008-0159-9
28. Sasaki Y, Towhata I, Miyamoto K, Shirato M, Narita A, Sasaki T, Sako S (2012) Reconnaissance report on damage in and around river levees caused by the 2011 off the Pacific coast of Tohoku earthquake. Soils Found 52(5):1016–1032
29. Sato S (2013) 2011 Tohoku tsunami and future directions for tsunami disaster mitigation. In: Wang Z, Lee JHW, Gao J, Cao S (eds) Proceedings of the 35th IAHR world congress, Chengdu, China, 8–13 September, invited keynote (CD-ROM)
30. Tanaka H, Nguyen XT, Umeda M, Hirao R, Pradjoko E, Mano A, Udo K (2012a) Coastal and estuarine morphology changes induced by the 2011 Great East Japan earthquake tsunami. Coast Eng J 54(1), paper 1250010. doi:10.1142/S0578563412500106
31. Tanaka N, Yagisawa J, Yasuda S (2012b) Characteristics of damage due to tsunami propagation in river channels and overflow of their embankments in Great East Japan earthquake. Int J River Basin Manag 10(3):269–279

32. Tanaka H, Adityawan MB, Udo K, Mano A (2014) Breaching and tsunami water drainage at old river mouth locations during the 2011 tsunami. In: Proceedings of the 34th international conference of coastal engineering, ASCE-KSCE, Seoul, Korea
33. Van Kessel T, Blom C (1998) Rheology of cohesive sediments: comparison between a natural and an artificial mud. J Hydraul Res IAHR 36(4):591–612
34. Viollet PL, Chabard JP, Esposito P, et Laurence D (2002) Mécanique des Fluides Appliquée. Ecoulements Incompressibles dans les Circuits, Canaux et Rivières, autour des Structures et dans l'Environnement ('applied fluid mechanics. Incompressible flows in pipes, channels and rivers, around structures and in the environment'), 2ème édition. Presses des Ponts et Chaussées, Paris
35. Wilson RI, Admire AR, Borrero JC, Dengler LA, Legg MR, Lynett P, Mccrink TP, Miller KM, Ritchie A, Sterling K, Whitmore PM (2013) Observations and impacts from the 2010 Chilean and 2011 Japanese tsunamis in California (USA). Pure Appl Geophys 170:1127–1147. doi:10.1007/s00024-012-0527-z
36. Yasusa H (2010) One-dimensional study on propagation of tsunami wave in river channels. J Hydraul Eng ASCE 136(2):93–105